Deep-Sea Research I 56 (2009) 1742–1756

Contents lists available at ScienceDirect

Deep-Sea Research I

journal homepage: www.elsevier.com/locate/dsri

Mesoscale distribution of zooplankton biomass in the northeast Atlantic Ocean determined with an Optical Plankton Counter: Relationships with environmental structures

Jean-Philippe Labat [a,b,*], Stephane Gasparini [a,b], Laure Mousseau [a,b], Louis Prieur [a,b], Marc Boutoute [a,b], Patrick Mayzaud [a,b]

[a] UPMC Univ Paris 06, UMR 7093, LOV, Observatoire océanologique, F-06230 Villefranche-sur-Mer, France
[b] CNRS, UMR 7093, LOV, Observatoire océanologique, F-06230 Villefranche-sur-Mer, France

ARTICLE INFO

Article history:
Received 6 February 2008
Received in revised form
12 May 2009
Accepted 22 May 2009
Available online 2 June 2009

Keywords:
Zooplankton
Biomass
Size distribution
Mesoscale eddies
Optical plankton counter
Pelagic environment
Northeast Atlantic Ocean

ABSTRACT

We examined the mesoscale distribution of zooplankton populations using a continuous recording system: the optical plankton counter (OPC). Data were collected in the mid-latitude northeast Atlantic inter-gyre region in April and September 2001 during the POMME 2 and POMME 3 cruises. This sector of the North Atlantic system is characterized by subduction phenomena and mesoscale eddies. Estimated mean biomass was 2.88 DW g m^{-2} in April and 1.64 DW g m^{-2} in September with populations dominated by small copepods of the genera, *Clausocalanus*, *Paracalanus* and *Oithona*. Day–night changes in vertical distribution appeared to be seasonally variable. During April, absolute concentrations within the upper layer above 50 m were higher at night. During September, vertical profiles of relative biomass were quite similar for day and night. Highest depth-integrated biomasses were located mainly on the periphery of anticyclonic eddies, with maxima related to the increase in depth range of vertical distribution. This pattern suggested that maximum biomass was associated with the most dynamic parts of the frontal features. Other zones of high zooplankton biomass were associated with the centers of cyclonic eddies and high fluorescence values. Using a 3D view, we found that zooplankton distribution showed a more complex pattern than in a 2D view with variable vertical distribution. Hence, proper description of the distribution of zooplankton underlines the need to describe this submesoscale with an order of magnitude around 10 nautical miles.

1. Introduction

Zooplankton play a key role in the control of phytoplankton production and are a critical food source for upper trophic levels, thus structuring pelagic ecosystems. Knowledge of changes in size structure of zooplankton communities has long been recognized as essential to understanding population dynamics (Sheldon et al., 1972; Vidal and Whitledge, 1982; Havens, 1998). To characterize pelagic ecosystems quantitatively, it is important to have robust estimates of biomass at different spatial scales. Traditionally, net tows are used to study zooplankton communities (biomass, species composition). However, they are often poorly suited because of spatial heterogeneity. Hence, integration of data at different scales is difficult. This is particularly true when measurements of zooplankton biomass are expected to show patchiness, such as in areas with contrasting hydrologic structures. The use of a continuous recording system such as the

* Corresponding author at: Observatoire Océanologique de Villefranche-sur-mer, BP28, 06234 Villefranche Cedex, France.
Tel.: +33 4 93 76 38 45; fax: +33 4 93 76 38 48.
E-mail address: jean-philippe.labat@obs-vlfr.fr (J.-P. Labat).

0967-0637/$ - see front matter © 2009 Elsevier Ltd. All rights reserved.
doi:10.1016/j.dsr.2009.05.013

Optical Plankton Counter (OPC) (Herman, 1988, 1992) is an alternative to net tows to characterize, at different scales, abundance and size distribution of zooplankton (Herman et al., 1993; Huntley et al., 1995; Kato et al., 1997; Mullin and Cass-Calay, 1997; Osgood and Checkley, 1997; Wieland et al., 1997; Currie et al., 1998; Grant et al., 2000; Huntley et al., 2000).

The work described here was part of a description of a North Atlantic system characterized by subduction structures and mesoscale eddies (French JGOFS program POMME: Program Ocean Multidisciplinaire Meso Echelle), where process studies were conducted over distinct seasons (September 2000–September 2001). This area is in the mid-latitude northeast Atlantic inter-gyre region, away from major current systems. In the upper layers, at the level of the North Atlantic Central Water (NACW), it is bound, to the north and northwest, by extensions of the North Atlantic Current (NAC) system, and to the south and southwest, by the Azores Current (Le Cann et al., 2005). The aim of this work is to describe the distribution of zooplankton biomass and the relationship with meso- and submesoscale structures.

2. Materials and methods

Distribution of the zooplankton populations was studied using a continuous recording system: the Optical Plankton Counter fitted on a Seasoar vehicle. Distribution of zooplankton biovolumes by size was recorded between 250 μm and 1 cm of equivalent spherical diameter (ESD). Hydrological parameters and chlorophyll distributions were simultaneously recorded with Seabird SBE 911 and WetStar sensor, respectively, fitted on the Seasoar. Vertical calibration nets tows were made with WP II nets (200 μm mesh size) to estimate biomass and to identify the main taxa.

2.1. OPC records

2.1.1. OPC use

The design, calibration and mode of operation of the OPC have been fully described by Herman (1988, 1992). Briefly, the OPC consists of a flow-through tunnel. Particles passing through the tunnel cross a rectangular light beam, the attenuation of which is proportional to the size of the particle. OPC-1T employs a narrow light beam of 4 mm width, 20 mm height and 220 mm length. Each particle going through this beam is viewed as a projected surface. Thus, the digital size recorded for a particle can be converted to a diameter, which is converted to the equivalent diameter of a sphere blocking the same amount of light as the particle (equivalent spherical diameter).

The OPC was towed at a speed between 7 and 10 knots in a saw-tooth undulating pattern over depths ranging between surface and ca. 300 m. In April, depth range was 10–340 m and the wavelength of any given oscillation was 1.4 nautical miles. In September the depth range was 1–260 m, and wavelength 1.1 nautical miles. Ship position was recorded every 2 s from a GPS system. Raw data sets were recorded over 1 h corresponding to 8 nautical miles.

OPC data acquisition software was used to convert signals from the underwater units into standard OPC text files. These raw data were transformed using specific software (TADO 7.1; Labat, unpublished). Size count data were pooled to categorize spatial unit cells delimited by predefined intervals with specific horizontal and vertical dimensions. The distance covered was computed from the position data. The volume of water passing through the OPC was estimated from this distance and the tunnel dimensions. Size distributions were expressed as volume per size class. The volume was calculated as parts per billion (ppb or $mm^3\,m^{-3}$). All unit cells are spatially localized by depth, latitude and longitude.

2.1.2. OPC sampling design

During the two POMME cruises using the Seasoar/OPC, #2 in April and #3 in September 2001, OPC transects were performed continuously in an area located between 38 and 45°N and between 16 and 21°W. Fig. 1 illustrates the OPC track for the different transects and grids for the two cruises, the locations of the calibration nets and the locations of the eddy centers. Nomenclature and location of eddies were described by monthly trajectories of eddy centers determined from Lagrangian-altimetry data (Le Cann et al., 2005).

Transects were planned to investigate different hydrological structures, particularly anticyclonic and cyclonic gyres. Analyses from operational models were available in near-real time (Assenbaum and Reverdin, 2005) and were used to determine ship tracks. They were obtained by objective analysis combining geostrophic velocity and float motion. In April, two 3D-grids linked by transect were investigated to obtain detailed spatial structure within and on the edge of the gyres. In the present study, we focussed on the south grid G1 where the frontal structure was clearly visible between a cyclonic (C4) and an anticyclonic (A2) gyre (Fig. 1). This zone between A2 and C4 corresponded to a zonal jet with peak velocities of $30\,cm\,s^{-1}$ and is one of the most important structures for the upper ocean dynamics in the POMME area (Paci et al., 2005). Additional transects, T10 and T20, and north grid, G2, where OPC data did not permit accurate resolution of spatial structure, were used only for estimates of total biomass and OPC biovolumes vs net biomass relationships. In September, transects crossed the different gyres in a 2D-type description from the north part to the south part of the POMME area.

2.1.3. OPC data analysis and spatial representation

From the unit cells, spatially localized by depth, latitude and longitude, interpolation of biomass was achieved using 2D and 3D grids by a triangle-based linear interpolation method with a horizontal step of 3 nautical miles and a vertical step of 5 m. To normalize data between the two cruises, we use only data above 250 m depth. Numerical representations were developed using Matlab metalanguage.

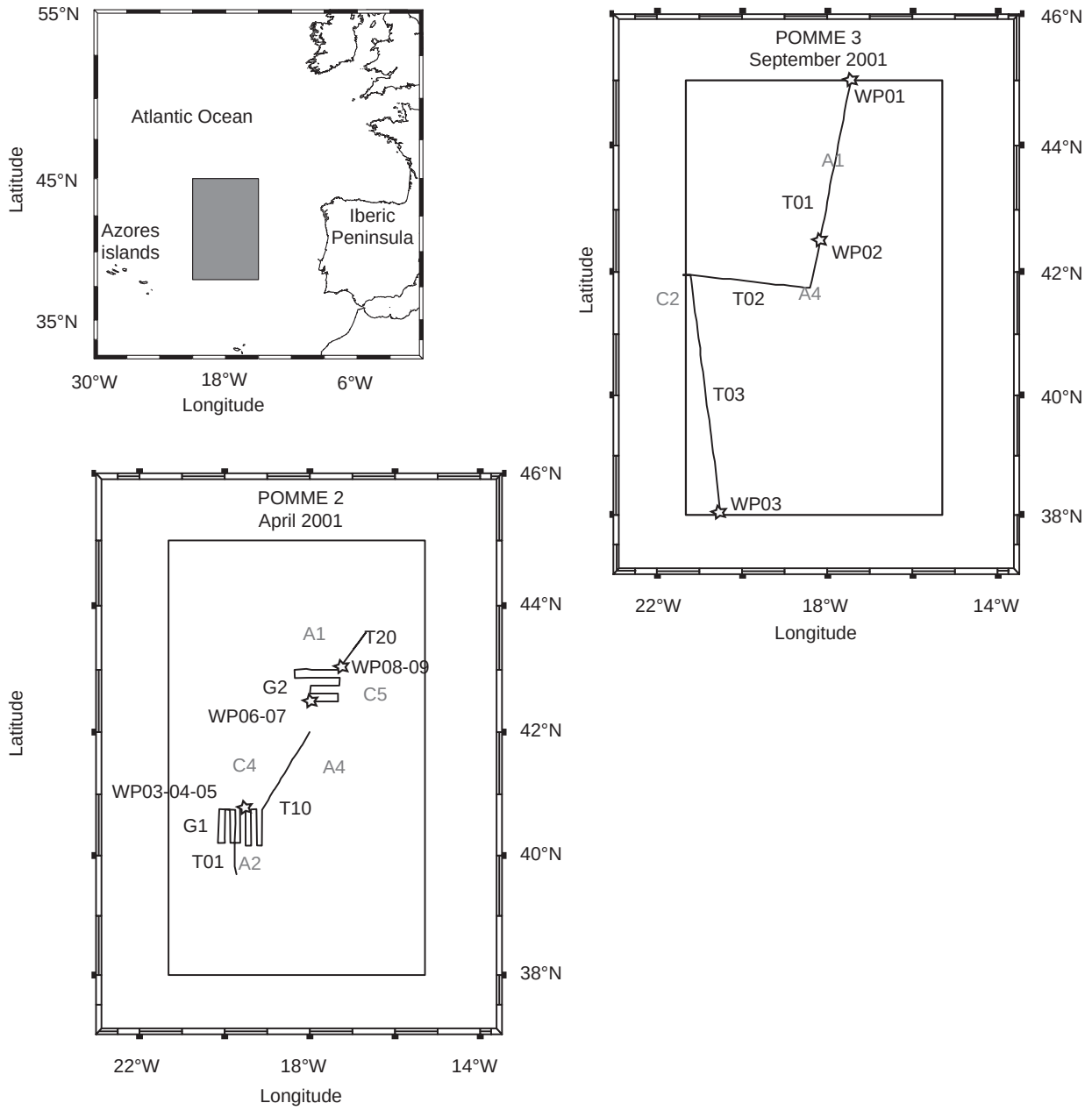

Fig. 1. Positions of transects (noted T) and grids (noted G) done with the OPC and station (calibration hauls) records during the POMME 2 and 3 cruises. Positions and labels of the nearest eddy centers (anticyclonic noted A and cyclonic C) are given from Le Cann et al. (2005).

2.1.4. Calibration net

Zooplankton samples were collected using a triple WP II net (0.25 m^2 surface aperture and 200 μm mesh size). Vertical hauls were made from ca. 200 m to the surface for eight stations and from 300 m for the remaining two (see Table 1). For each net haul, two samples were used for duplicate biomass measurement and the third one for taxonomic determination and enumeration. Biomass samples were filtered on 200 μm pre-weighted netting and rinsed with ammonium formate. The material was immediately frozen at −20 °C on board. Within 3 months, all samples were oven dried (48 h at 60 °C) at the laboratory and weighed. Total weight is expressed in milligrams of dry weight per cubic meter (DW mg m^{-3}) and in gram of dry weight per square meter (DW g m^{-2}).

Taxonomic samples were preserved immediately after the net tow with 5% buffered formaldehyde. Species determinations and enumerations were made using a binocular microscope. Size and ESD were measured on ten individuals of each dominant taxon using a Visiolab 1000 video analysis system (Biocom). To estimate a Biovolume-to-Biomass Conversion function (BBC function), each biomass value in DW g m^{-2} was related to the biovolume in cm^3 m^{-2}, averaged over the nearest OPC initial set of

Table 1
Number ($n\,m^{-3}$) and biomasses ($DW\,g\,m^{-2}$) estimated by net haul and number ($n\,m^{-3}$) and biovolume ($cm^3\,m^{-2}$) recorded by OPC near the haul location. Biomass/biovolume ratios are given for each haul.

	Haul	Date		Cable length (m)	Net number ($N\,m^{-3}$)	Net 1 biomass ($DW\,g\,m^{-2}$)	Net 2 biomass ($DW\,g\,m^{-2}$)	Net average ($DW\,g\,m^{-2}$)	Net average ($DW\,mg\,m^{-3}$)	Number (nm^{-3})	OPC biovolume ($cm^3\,m^{-2}$)	Biomass on biovolume ratio
POMME 2												
Station 1	WP03	19/04/2001	Night	300	720	1.98	1.83	1.91	9.5	913	15.8	0.121
Station 1	WP04	19/04/2001	Night	200	1380	2.62	2.64	2.63	14.6	913	15.8	0.167
Station 1	WP05	19/04/2001	Night	200	852	2.65	2.54	2.60	14.4	913	15.8	0.164
Station 2	WP06	22/04/2001	Night	200	689	2.86	2.10	2.48	12.1	876	17.8	0.139
Station 2	WP07	22/04/2001	Night	200	ND	2.96	3.08	3.02	15.1	876	17.8	0.170
Station 3	WP08	23/04/2001	Day	300	271	2.08	2.07	2.07	10.4	856	17.3	0.120
Station 3	WP09	23/04/2001	Day	200	398	2.05	2.15	2.10	10.0	856	17.3	0.121
POMME 3												
Station 1	WP01	09/09/2001	Night	200	322	2.40	2.42	2.41	13.4	793	19.0	0.127
Station 2	WP02	10/09/2001	Night	200	240	1.05	1.89	1.47	8.6	480	9.6	0.154
Station 3	WP03	13/09/2001	Night	200	ND	1.40	0.80	1.10	6.9	543	11.4	0.096

data (around 8 nautical miles). OPC biovolumes were integrated through a standard depth of 250 m. Significance of correlation coefficients and slope parameters of the function were computed by a bootstrap method.

3. Results

3.1. Net biomass

Integrated biomasses were estimated from ten triple-net hauls, seven from the POMME 2 cruise at three stations and three from the POMME 3 cruise at three stations. The numbers and the biomasses from each net are presented in Table 1. Mean net biomass was higher in April ($n = 14$, mean $= 2.40\,DW\,g\,m^{-2}$) than in September ($n = 6$, mean $= 1.66\,DW\,g\,m^{-2}$) (Wilcoxon rank test, $P = 0.0288$). Differences between night and day and between 200 and 300 m vertical hauls could not be statistically tested but appears negligible, within the variability between nets at the same place.

3.2. Taxonomic results

Species abundances are given for eight vertical hauls, six from the POMME 2 cruise at three stations (Table 2A) and two from the POMME 3 cruise at two stations (Table 2B). Minimum and maximum ESD are also given for each taxon. The dominant taxonomic groups are represented by the small copepods of the genera *Clausocalanus*, *Paracalanus* and *Oithona*. In September, the genera *Centropages* and *Acartia* are also well represented, and larger organisms such as Appendicularia and Ostracods showed higher frequency than in April.

3.3. Biovolume by OPC operations

Distance and duration of OPC transects and grids are given in Table 3. The average biovolumes ($mm^3\,m^{-3}$) and the spectra of biovolumes per size class are shown in Fig. 2 for each operation of both POMME 2 and POMME 3. Considering size classes separately, most of the biovolumes were higher in April than in September, particularly for the small size range. In this latter case, the differences were probably associated with the changes in *Paracalanus parvus* abundance.

The mean values recorded for the entire size range corresponded to biovolumes ranging from 75.32 to $96.10\,mm^3\,m^{-3}$ in April, and to biovolumes ranging from 45.31 to $51.68\,mm^3\,m^{-3}$ in September. Within the April spectra, the maximum values (T01: $81.09\,mm^3\,m^{-3}$, G1: $81.06\,mm^3\,m^{-3}$, T10: $84.60\,mm^3\,m^{-3}$, G2: $96.10\,mm^3\,m^{-3}$) are also characterized by a dominance of the size classes between 1.5 and 2.5 mm ESD. Conversely, the lowest April value (T20: 75.32 $09\,mm^3\,m^{-3}$), located on the northern part of the POMME zone, is characterized by relatively weak values for this size class.

Among the dominant taxa of this size range, *Mesocalanus tenuicornis* and *Euchirella rostrata* were those showing the most important changes in abundance from one operation to another (Table 2A).

Table 2
Frequencies for the most numerous taxonomic groups for small copepods, large copepods and other taxa.

(A) For POMME 2 cruise

POMME 2 south area			ESD (mm)	
		%	Min	Max
WP03	**720 ind m^{-3}**			
Small copepods				
Clausocalanus sp.1	Female	27.49	0.35	0.50
Clausocalanus sp.1	Juvenile	19.68	0.35	0.50
Paracalanus parvus	Female	11.86	0.60	0.65
Oithona spp.	Female	9.16	0.30	0.50
Clausocalanus sp.2	Female	8.88	0.65	0.95
Paracalanus parvus	Juvenile	7.82	0.50	0.65
Large copepods				
Mesocalanus tenuicornis	Juvenile	4.11	1.05	1.75
Euchirella rostrata	Juvenile	1.97	2.10	2.35
Mesocalanus tenuicornis	Female	1.61	2.15	2.25
Others (mainly ostracods, salps)		3.92	–	–
WP04	**1380 ind m^{-3}**			
Small copepods				
Clausocalanus spp.	Juvenile	25.97	0.35	0.50
Paracalanus parvus	Juvenile	17.31	0.50	0.65
Clausocalanus spp.	Female	16.23	0.35	0.50
Paracalanus parvus	Female	13.91	0.60	0.65
Oithona spp.	Juvenile	5.10	0.35	0.40
Oithona spp.	Female	4.33	0.40	0.50
Large copepods				
Mesocalanus tenuicornis	Juvenile	0.22	1.05	1.75
*Paraeuchaeta tonsa**	Juvenile	0.13	3.01	3.61
*Calanus helgolandicus**	Juvenile	0.12	1.38	2.05
Others (mainly appendicularians)		0.48	–	–
WP05	**852 ind m^{-3}**			
Small copepods				
Clausocalanus sp.1	Juvenile	32.12	0.35	0.50
Paracalanus parvus	Juvenile	19.68	0.40	0.60
Clausocalanus sp.1	Female	14.76	0.50	0.60
Paracalanus parvus	Female	9.12	0.50	0.70
Oithona spp.	Juvenile	3.18	0.30	0.45
Clausocalanus sp.1	Male	2.89	0.35	0.45
Large copepods				
Euchirella rostrata	Juvenile	0.25	2.10	2.35
Mesocalanus tenuicornis	Juvenile	0.19	1.05	1.75
Pleuromamma piseki	Female	0.17	1.00	1.40
Others (mainly appendicularians)		0.86	–	–

POMME 2 north area			ESD (mm)	
		%	Min	Max
WP06	**689 ind m^{-3}**			
Small copepods				
Clausocalanus sp.1	Juvenile	34.48	0.35	0.50
Clausocalanus sp.1	Female	27.01	0.35	0.50
Paracalanus parvus	Juvenile	11.58	0.40	0.50
Clausocalanus sp.2	Juvenile	4.37	0.65	0.80
Paracalanus parvus	Female	3.34	0.40	0.55
Large copepods				
*Calanus helgolandicus**	Juvenile	0.36	1.38	2.05
Euchaeta sp.	Juvenile	0.27	2.10	2.35
Mesocalanus tenuicornis	Juvenile	0.23	1.05	1.75
Others (mainly ostracods)		0.72	–	–
WP08	**271 ind m^{-3}**			
Small copepods				
Clausocalanus sp.1	Juvenile	32.73	0.35	0.55
Oithona spp.	Female	15.52	0.40	0.50
Oithona spp.	Juvenile	11.22	0.30	0.40

Table 2 (*continued*)

POMME 2 north area				
		%	ESD (mm) Min	Max
Clausocalanus sp.1	Female	6.76	0.45	0.60
Paracalanus parvus	Juvenile	6.30	0.40	0.50
Paracalanus parvus	Female	5.38	0.40	0.55
Clausocalanus sp.2	Juvenile	4.76	0.65	0.80
Large copepods				
Heterorhabdus sp.	Juvenile	0.36	2.10	2.35
Euchirella rostrata	Female	0.27	2.00	4.70
Euchaeta sp. C5	Juvenile	0.20	–	–
Others (mainly chaetognaths, ostracods)		1.19	–	–
WP09	**398 ind m^{-3}**			
Small copepods				
Clausocalanus sp.1	Juvenile	35.02	0.35	0.55
Oithona spp.	Female	16.62	0.35	0.50
Oithona spp.	Juvenile	8.88	0.30	0.40
Clausocalanus sp.1	Female	6.45	0.45	0.60
Paracalanus parvus	Juvenile	6.29	0.40	0.50
Paracalanus parvus	Female	5.65	0.40	0.55
Clausocalanus sp.2	Juvenile	3.39	0.65	0.80
Large copepods				
Euchirella rostrata	Female	1.30	2.10	2.35
*Paraeuchaeta norvegica**	Juvenile	0.54	3.75	4.77
Mesocalanus tenuicornis	Juvenile	0.31	1.05	1.75
Others (mainly chaetognaths, ostracods)		1.19	–	–

(B) For POMME 3 cruise

POMME 3			ESD (mm)	
		%	Min	Max
WP01	**322 ind m^{-3}**			
Small copepods				
Clausocalanus sp.1	Juvenile	46.27	0.40	0.55
Centropages typicus	Juvenile	15.53	0.47	0.58
Clausocalanus sp.1	Female	13.22	0.45	0.60
Centropages typicus	Female	7.60	0.65	0.80
Clausocalanus sp.1	Male	2.97	0.40	0.55
Acartia clausi	Female	2.97	0.40	0.85
Centropages typicus	Male	1.65	0.60	0.80
Large copepods				
Pleuromamma sp.	Juvenile	1.32	–	–
*Euchaeta acuta**	Juvenile	1.32	1.94	2.53
*Nannocalanus minor**	Juvenile	0.66	0.85	1.34
Others (Appendicularian, ostracods, chaetognaths)		7.40	–	–
WP02	**240 ind m^{-3}**			
Small copepods				
Clausocalanus sp.1	Juvenile	24.49	0.40	0.55
Acartia plumosa	Female	19.43	0.50	0.55
Clausocalanus sp.1	Female	12.90	0.45	0.60
Clausocalanus sp.2	Female	7.51	0.65	0.80
Centropages typicus	Female	3.24	0.60	0.80
Centropages typicus	Male	2.71	0.60	0.80
Acartia plumosa	Male	2.12	0.65	0.75
Centropages typicus	Juvenile	2.12	0.65	0.80
Clausocalanus sp.2	Juvenile	1.80	0.55	0.70
Clausocalanus sp.2	Male	1.47	0.55	0.70
Oithona spp.	Juvenile	1.31	0.30	0.40
Acartia plumosa	Juvenile	1.14	0.30	0.45
Large copepods				
Nannocalanus minor	Female	0.82	0.85	1.35
Mesocalanus tenuicornis	Juvenile	0.77	1.05	1.75
Mesocalanus tenuicornis	Female	0.73	2.15	2.25
Others (ostracods)		4.95	–	–

Ranges of the ESD are given for the copepods by direct sizing or for any species labelled by * from Razouls et al. (2005–2008).

Table 3
Distance and length of the day and night sampling during transects and grid for the two cruises.

	Duration	Distance (nautical miles)		
		Total	During day	During night
POMME 2				
Transect T01	7h30	63	34	29
Grid G1	46h00	399	238	161
Transect T10	9h00	76	0	76
Grid G2	30h30	226	123	103
Transect T20	6h30	52	38	14
Total	99h30	816	429	387
POMME 3				
Transect T01	29h30	201	99	102
Transect T02	17h30	139	23	116
Transect T03	29h30	229	123	106
Total	76h30	569	250	319

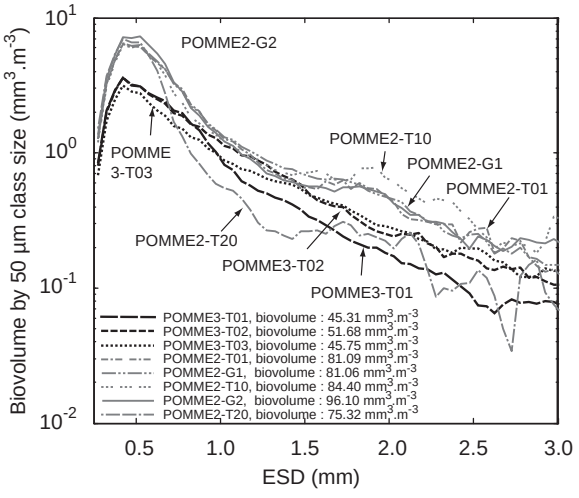

Fig. 2. Biovolume ($mm^3\,m^{-3}$) distribution by size using a 50 µm class interval for OPC transects and grids. Total biovolumes are given for each operation.

September spectra and biomass values were less variable than in April. Only the northern transect (T01) differed slightly from the others by showing the least biovolume in the 1–3 mm size range.

Finally, the overall pattern of biovolume distribution by size classes is likely related to the effect of two components: (i) season with opposition between spring and summer and (ii) latitude with lower proportions of large size classes in northern areas.

3.4. Biovolume-to-Biomass Conversion function

Table 1 shows the biomass values measured in duplicate from the ten net hauls. Biomass and OPC volumes recorded simultaneously were significantly correlated (R: 0.6980, $P = 0.0025$ by bootstrap estimation). A linear regression (Fig. 3) has been fitted to define a

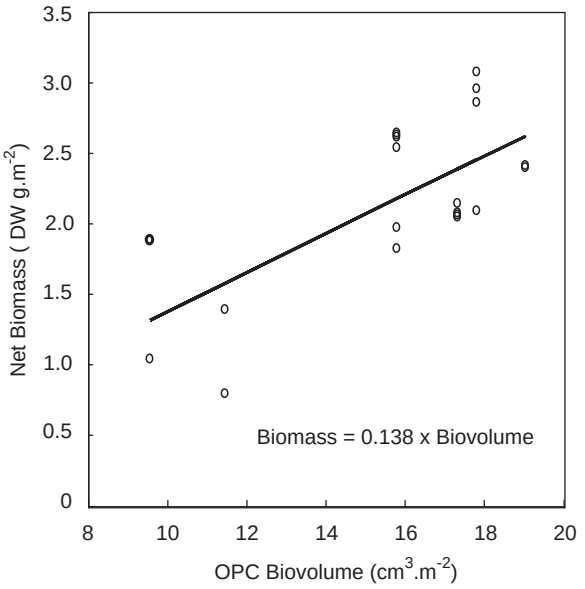

Fig. 3. Relationship between calibration net biomasses (dry weight in $DW\,g\,m^{-2}$) and OPC biovolume ($cm^3\,m^{-2}$) recorded near each net haul.

Biovolume-to-Biomass Conversion function (Biomass = a Biovolume) between net biomass ($g\,DW\,m^{-2}$) and OPC volume ($cm^3\,m^{-2}$). A value of 0.138 for a was computed (95% limits are 0.1249–0.1508). This relationship was used to convert all biovolume values into dry weight.

3.5. Biomass from OPC operations

Fig. 4 shows the mean dry weights estimated from integrated biovolumes using the BBC function (above), for the three transects and the two grids of POMME 2 and the three transects of POMME 3 cruises. The values recorded for POMME 2 ranged between 2.59 and 3.31 $g\,DW\,m^{-2}$. As expected, values for the T01 transect and the G1 grid are very similar, since they describe the same area. For POMME 3 values ranged between 1.56 and 1.78 $g\,DW\,m^{-2}$. Mean biomass for the two cruises varied from 2.88 $g\,DW\,m^{-2}$ for POMME 2 in April to 1.64 $g\,DW\,m^{-2}$ for POMME 3 in September. These values are significantly different (Wilcoxon test, $P<0.05$).

3.6. Day/night vertical distribution patterns

Day and night vertical distributions for each of the two cruises were computed by integrating all data recorded during day and night for both seasons. Integration factors (survey distance and duration of transects for day and night periods) are indicated in Table 3 for the two cruises. These integrations yielded a mean vertical distribution for POMME 2 based on 816 nautical miles and 99h30 (more than 4 day/night cycles) and for POMME 3 on 569 nautical miles and 76h30 (more than 3 day/night cycles). During POMME 2, the integrated biomass values for night (2.86 $g\,DW\,m^{-2}$) and day (2.82 $g\,DW\,m^{-2}$) were similar, but the vertical distributions showed higher values at night within the upper layer above 50 m associated with a lower

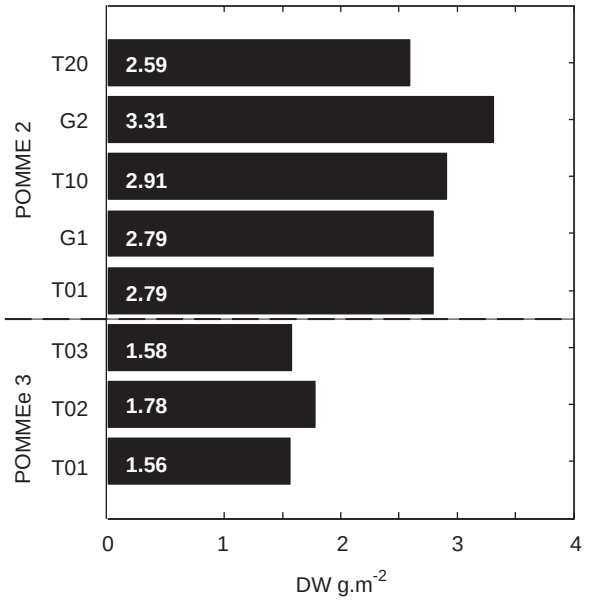

Fig. 4. Biomasses (dry weight in DW g m^{-2}) for POMME 2 (3 transects and 2 grids) and POMME 3 (3 transects).

biomass below 50 m (Fig. 5). Relative distribution displayed the same relationship (Fig. 5). During POMME 3, the integrated biomass at night was overall higher (1.92 g m^{-2}) than during the day (1.55 g m^{-2}), but the vertical profiles of relative biomass were quite similar for both day and night.

3.7. Transects and grid data

3.7.1. April cruise (POMME 2)

Simultaneous spatial distribution (2D and 3D) of the biomass and of environmental parameters (temperature and fluorescence) was available only for T01 transect and G1 grid. Joint analysis for transects T10, T20 and grid G2 was not possible because of irregular sampling of the different parameters.

The area, described by T01 and G1, was intensively investigated in order to study the submesoscale structure between the anticyclonic eddy, A2 centered on 39.8°N and 19.6°W, and the cyclonic eddy, C4 centered on 41.3°N and 19.3°W (Le Cann et al., 2005). The locations of anticyclonic and cyclonic mesoscale eddies were found during POMME Leg 1 CTD station arrays. The eddies moved slowly because of their deep density signature (down to 2000 m).

Fig. 6 presents the data for fluorescence, temperature and biomass along transect T01 in 2D representation and for the grid G1 in 3D representation. A part of the transect T01, north of 41.1°, is included in the grid pattern (see T01 in dotted line on the location map, Fig. 6). Fig. 8A presents the distribution in number for the T01 transect for the three size classes.

Variations of the isotherms showed hydrologic structures with the 14 °C isotherm below 150 m in the southern part and near 50 m in the northern part. Between these two features, a frontal structure between 40.2°N and 40.4°N latitude is clearly visible with a sharp vertical component of the 14 °C isotherm (Fig. 6). This corresponds to the thermal signature of the density changes between the anticyclonic and the cyclonic zones, respectively, south and north of the frontal structure.

A strong zonal eastward current marked this frontal area, as shown by the ADCP data (Legal et al., 2007). Higher salinity and temperature near the surface were also recorded by CTD, just south of the frontal zone (between 40.15° and 40.35°N) over 20 nautical miles. Hence, this area is characterized by very dynamic processes with a geostrophic advective effects and contrasted vertical velocity in the range of a few m day^{-1} (Giordani et al., 2006; Legal et al., 2007). Distribution of fluorescence showed a subsurface maximum with high values of fluorescence in the north and south areas and low values in the middle zone (Fig. 6) corresponding to this particular structure.

Zooplankton biomass was maximal near the surface (between 0 and 50 m) in all areas. The higher integrated zooplankton biomass appeared located in the southern part of the frontal zone, resulting from a wider vertical extension of the population distribution. The same pattern is viewed from the distribution in number (Fig. 8A). This maximum of integrated zooplankton biomass was also clearly associated with the lowest fluorescence values. The low chlorophyll biomass/high integrated zooplankton biomass area, between 40.1° and 40.37°N, corresponded to physical structures linked with higher salinity, higher temperature and inversion of the sign of vertical velocities over a distance of a few kilometers.

Using a 3D view of the same hydrological area (grid G1), it can be seen that the northern area showed a shoaling of the 14 °C isotherm associated with high values of fluorescence and a frontal zone marked by a sinking of the isotherm and low fluorescence values (Fig. 6). This view extends the previous description with an east–west dimension. The zooplankton biomass distribution showed a more complex pattern than in the 2D view: the increase in concentrations with depth was not regular in the 3D view but rather showed patchy structures within the 10–15 nm radius. As in the 2D view, the integrated biomass displayed a maximum in the southern part of the frontal structure with values surpassing 4 g DW m^{-2} in contrast with the northern area (particularly the west part) where values below 2 g DW m^{-2} were observed. The subsurface maxima areas were not related to areas of maximum integrated biomass. Two different patterns were observed: (i) a high zooplankton biomass near the surface linked with subsurface fluorescence maximum and (ii) a high integrated zooplankton biomass, due to a larger vertical range of the zooplankton biomass linked with low fluorescence values in the south. This second pattern is clearly linked with a highly dynamic physical structure at the submesoscale described above.

3.7.2. September cruise (POMME 3)

In September, temperature ranged between 15 and 18/20 °C and was structured as a strong vertical stratification, marked by a thermocline between 50 and 100 m (Fig. 7). The 15 °C isotherm, the lower limit of the thermocline,

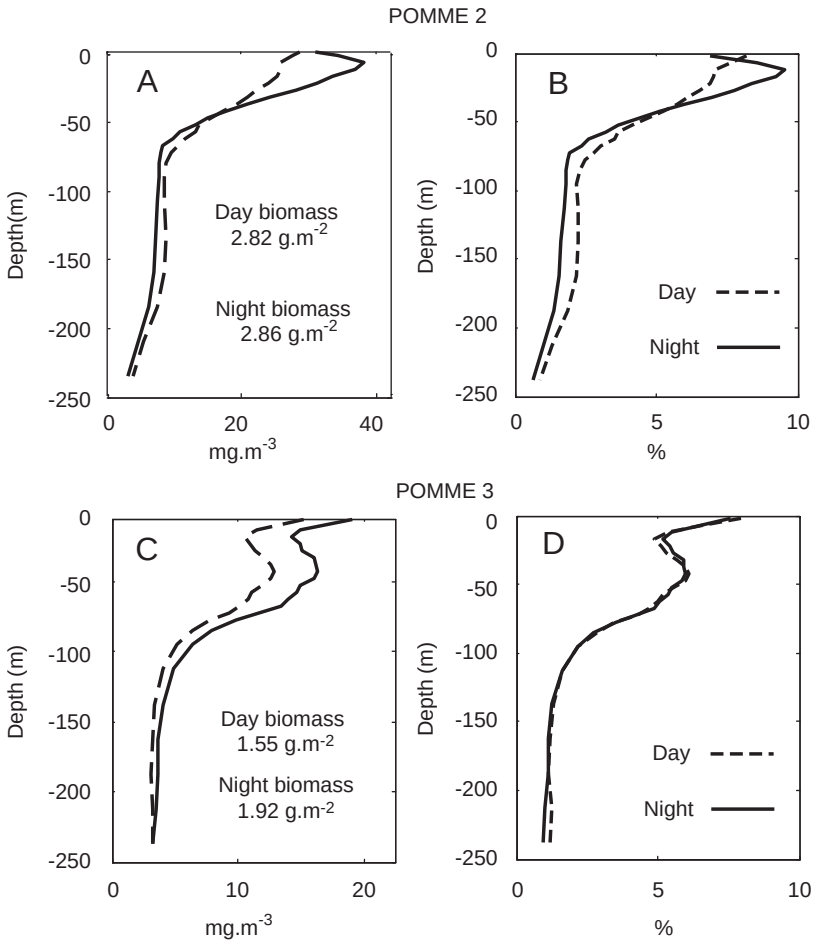

Fig. 5. Vertical distributions of the zooplankton biomasses for day (dotted line) and night (continuous line) periods integrated for all POMME 2 operations and for all POMME 3 operations. A and C = absolute dry weight in mg DW m^{-3} and B and D = relative dry weight (% of the sum of the integrated biomass for each profile).

sank from the northern to the southern part of the sampled zone. Only in the northern area did temperatures less than 20 °C reach the surface. Fluorescence distribution showed a maximum between 50 and 100 m, corresponding approximately with the 15 °C isotherm, both within and on the edge of the gyres.

In transects T01, T02 and T03, zooplankton biomass was distributed mostly within the 0–100 m layer, with highly localized areas of high concentration around 50 m depth associated with an increase of the depth range distribution. These areas corresponded with maxima of integrated biomass and were located mainly in the outer parts of eddies. Fig. 8(B–D) shows the distribution of the zooplankton expressed by numbers for the three size classes. These distributions are consistent with the data expressed by biomass.

On the T01 transect, the upper layer (0–250 m) signature of the A1 eddy, centered at 43.9° N and 18.0°W (Le Cann et al., 2005) and characterized by the vertical pattern of the 13° and 14° isotherms, is confusing: north of the estimated center, around 44.35° and 44.7°N, two areas showed a deeper 13 °C isotherm, associated with higher salinity (data not shown). These areas are separated by a zone around 44.5°N showing rising isotherm and lower salinity. These observations probably indicate complex small-scale dynamic processes. In this area, the maximum integrated zooplankton biomass was observed in the zone associated with low fluorescence values.

In the same T01 transect, the northern margin between the A4 anticyclonic eddy and C5 (42.7°N, 17.5°W) cyclonic eddies (Le Cann et al., 2005) at 42.5–42.7°N displayed an important vertical gradient associated with the 13° and 14° isotherms (Fig. 6) and isohaline profiles (data not shown). The zooplankton biomass located near this zone was associated with the cyclonic eddy and with higher values of fluorescence.

On the T02 transect, the A4 eddy signature near the surface was unclear, and a maximum of zooplankton biomass, associated with low values of fluorescence, was recorded at 19.2°W. On the T03 transect, a maximum of zooplankton was observed around 41.30°N and was associated with high fluorescence in an area located in the central part of a cyclonic eddy, as shown by the

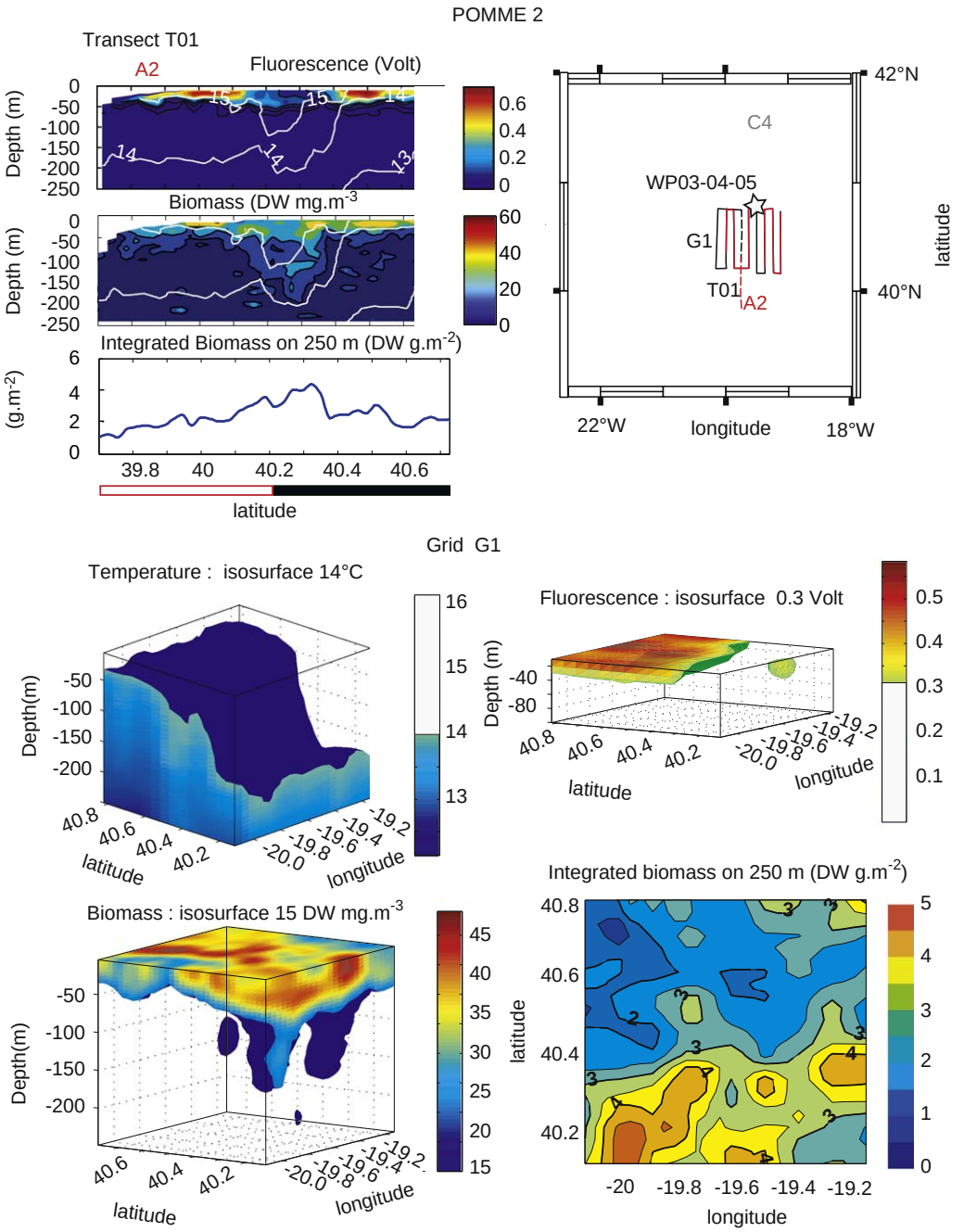

Fig. 6. POMME 2 cruise: distribution of isotherms (°C), fluorescence (relative units), zooplankton biomass (DW mg m^{-3}) and integrated biomass (DW g m^{-2}) for the T01 Transect in 2D view and the G1 grid in 3D view. For the 3D views, isotherm surface representations are used. A map summarizes the position of the OPC operations, the net samples (WP) and nearest eddy centers (Le Cann et al., 2005). Color bars give the night (black filled) and the day (red frame) periods. (For interpretation of the references to colour in this figure legend, the reader is referred to the web version of this article.)

isotherm shape (C2 at 41.5°N and 22.2°W; Le Cann et al., 2005).

The general pattern emerging from the data showed that in the anticyclonic eddies, the maxima of zooplankton biomasses are located on the edges and linked to low values of fluorescence. In contrast, the cyclonic eddy showed maximum biomass in the center, associated with high fluorescence values.

4. Discussion

4.1. OPC use

The Optical Plankton Counter has been used often to obtain data describing zooplankton spatial distribution (Huntley et al., 1995; Stockwell and Sprules, 1995; Kato et al., 1997; Osgood and Checkley, 1997; Grant et al., 2000;

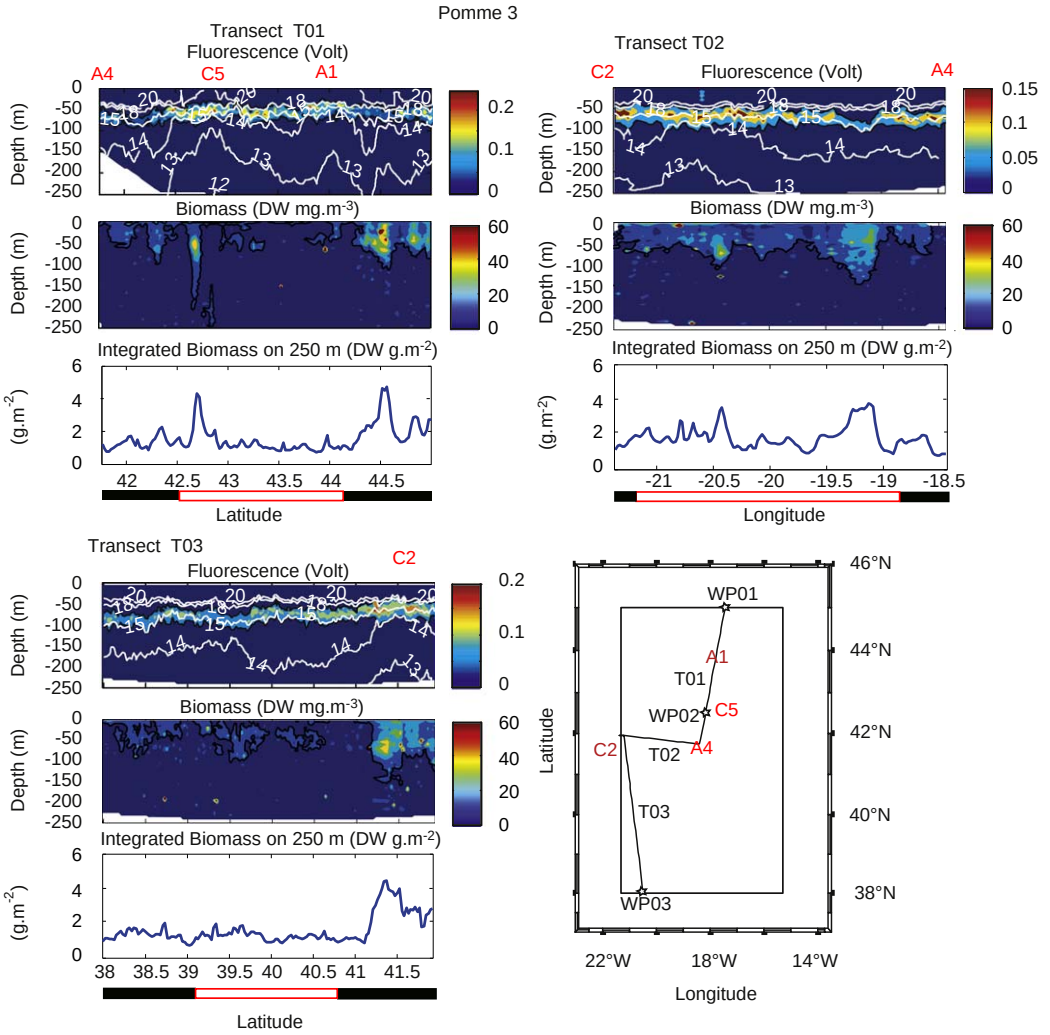

Fig. 7. POMME 3 cruise: distribution of isotherms (°C), fluorescence (relative units), zooplankton biomass (DW DW mg m^{-3}) and integrated biomass (DW g m^{-2}) for the 3 transects. A map summarizes the position of the OPC operations, the net samples (WP) and nearest eddy centers (anticyclonic noted A and cyclonic C) (Le Cann et al., 2005). Color bars give the night (black filled) and the day (red frame) periods. (For interpretation of the references to colour in this figure legend, the reader is referred to the web version of this article.)

Albaina and Irigoien, 2004). Comparison of OPC data with other sampling gears such as nets has yielded somewhat contradictory results (Sameoto et al., 1990; Sprules et al., 1998; Grant et al., 2000; Labat et al., 2002). Estimation of overall total zooplankton biomass and composition by the OPC may present technical limitations, particularly with regard to translucent organisms, coincident counts and inorganic particles. The biovolume of transparent organisms may be misread by the OPC, leading to an increased bias in size measurements when these organisms become abundant (Wieland et al., 1997; Beaulieu et al., 1999). However, in our study, transparent organisms were relatively poorly represented, the bulk of the catches comprising mainly copepods. Another possible bias may arise when two or more particles pass simultaneously through the detection beam and are thereby not resolved as separate objects. In some cases, coincident counting could be the major problem for an accurate estimate of zooplankton abundance (Sprules et al., 1992; Woodd-Walker et al., 2000; Remsen et al., 2004). However, during the POMME cruises, counts per second were less than 50 for the richest zone and averaged between 10 and 20 count s^{-1}, which is far below the minimum level at which coincidence is considered to become significant (Herman, 1992; Sprules et al., 1998; Heath et al., 1999; Woodd-Walker et al., 2000). Additionally, our study is based on biomass estimates, and the OPC yielded more accurate data than counts, as noted by Sprules et al. (1998). Another possible bias is the detection of inorganic particles (Heath et al., 1999; Halliday et al., 2001; Liebig et al., 2006). Nevertheless, in offshore pelagic ecosystems such as our study area, these particles represent a negligible fraction of the seston (Labat et al., 2002; Liebig et al., 2006). Moreover, the use of a biovolume-to-biomass conversion function built from biovolumes estimated by OPC and biomass estimated by net minimized the

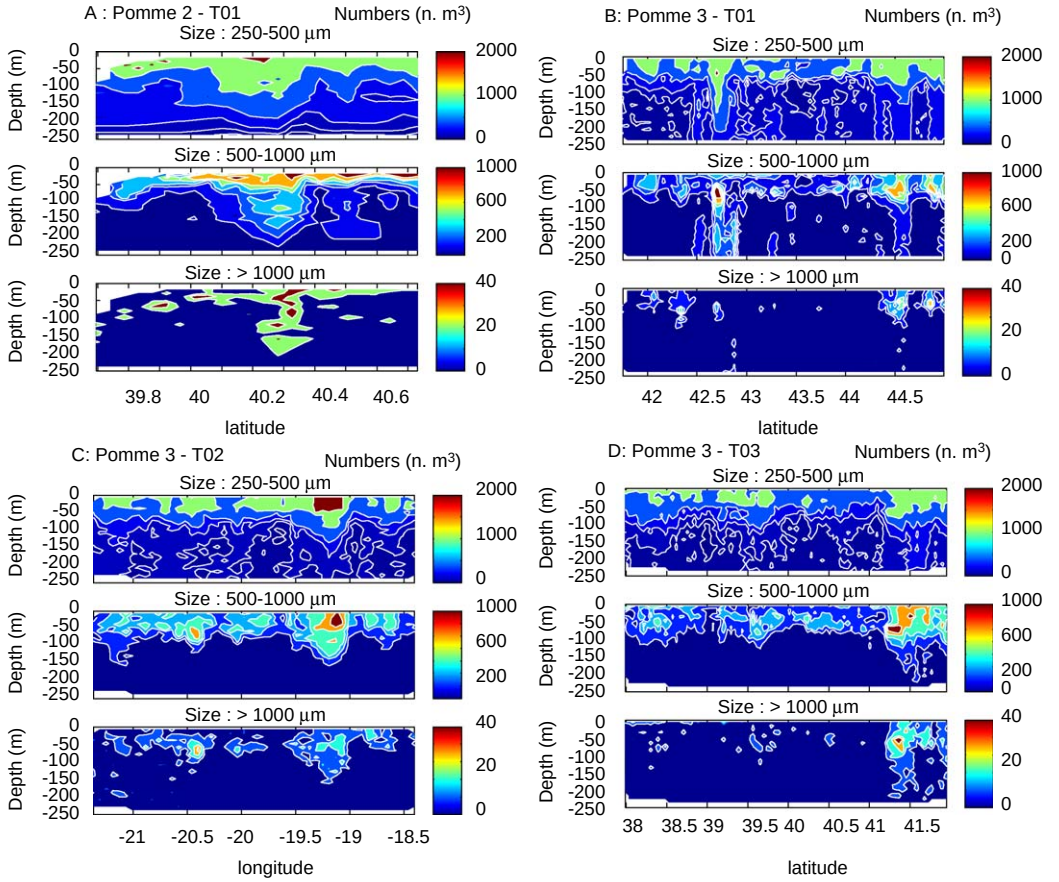

Fig. 8. Distribution in numbers ($n\,m^{-3}$) recorded by the OPC for three size classes (250–500 µm, 500–1000 µm, >1000 µm). A = POMME 2 cruise, transect T01. B, C, D = POMME 3 cruise, respectively transects T01, T02, T03.

problems associated with the inorganic particles and coincident counting. The remaining limitation lies with the use of net sampling for reference (Labat et al., 2002), which leaves open the potential bias of net sampling, such as the underestimation of the smaller size classes. Another potential error could arise from the presence of large phytoplankton aggregates. During the POMME cruises, the abundance and the composition of the phytoplankton (Claustre et al., 2005) suggested that this is not a significant source of error. Actually, the differences, sometime important but not systematic, between OPC counts and net counts reported in this study (Table 1) are likely to be the result of two effects: (i) a higher variability in net counts than in OPC counts, even at the same location and (ii) the ability of the OPC to detect small zooplanctic organisms that are not caught by 200 µm mesh size nets (Hopcroft, 2002; Labat et al., 2002).

4.2. Biovolume–biomass conversion

In the present study, we found a BBC function with a slope of 0.138. This value is similar to those computed or used in earlier studies: 0.13 (Lovegrove, 1966), 0.11 (Woodd-Walker et al., 2000), 0.119 (Gallienne et al., 2001), 0.16 (Finenko et al., 2003) and 0.126 (Patoine et al., 2006).

4.3. Overall biomass estimate

We measured mean dry weight, integrated over the survey grids and transects. The values ranged from 2.59 to 3.31 g DW m^{-2} (10.4–13.2 mg DW m^{-3}) in April and from 1.56 to 1.78 g DW m^{-2} (6.2–7 1 mg DW m^{-3}) in September. Our values agree with those reported in other studies in similar areas. For example, in an area of the eastern tropical Atlantic, south of the POMME zone, a mean annual estimation of 3.09 g DW m^{-2} was reported (Finenko et al., 2003). For Canary island eddies, values of 1.28 g C m^{-2} (3.3 g DW m^{-2}) inside and 0.58 g C m^{-2} (1.45 g DW m^{-2}) outside the eddy were recorded (Yebra et al., 2005). Within anticyclonic slope water in the Bay of Biscay, summer values between 1.3 and 1.6 g DW m^{-2} were recorded (Isla et al., 2004). Along the 20°W longitude and the same latitude, surface layers biomass ranged from 3 to 30 mg DW m^{-3} (Gallienne et al., 2001). In addition, their study reported lower biomass in September than in April and a dominance of the genus *Clausocalanus* throughout the cruise, with common occurrence of

Acartia, *Paracalanus* and *Oithona* species. An overall biomass estimate using acoustic sampling at 153 kHz showed, for the same area, lower values, 0.2–0.7 g m^{-2} (Wade and Heywood, 2001). The discrepancy is probably related to the difference in the zooplankton size fractions detected by the two methods.

4.4. Diel vertical migration

Several studies have shown that the vertical distribution of zooplankton is often determined by diel vertical migration (DVM), as an adaptive response based on a trade-off between maximum energy input and maximum protection (Lampert, 1989). DVM regulation by physical structures (stratification or not) and by the depth of the chlorophyll maximum characterises numerous patterns (Harris, 1988; Ashjian et al., 1998; Gray and Kingsford, 2003; Jiang et al., 2007). In our study, differences between the patterns of migration in April and in September could be viewed as a response to environments differently stratified (April was weakly stratified while September showed a strong stratification) and with contrasting phytoplankton biomasses. In April, we observed a vertical displacement of the maximum biomass of zooplankton associated with day/night cycles as well as with the subsurface chlorophyll maximum. In September, the chlorophyll maximum is below the thermocline (50–80 m), limiting the need of vertical displacement of migrating zooplankton.

The integrated biomass at night is higher than that during the day with a vertical profile of relative biomass quite similar for both day and night. This could be interpreted in two ways: (i) as an absence of daily vertical movement at the described scales and (ii) as a migration from below 250 m to the upper layer. The size distribution of the biomass (88% >2 mm, 98% <5 mm) strongly suggests than the major effect is due to an absence or a very small vertical migration during this period.

4.5. Eddy effects

The association between zooplankton distribution and physical structure such as cyclonic and anticyclonic eddies has been the object of various studies. Accurate description of mesozooplakton distribution relies mainly on the definition of the spatial scale considered. Mesoscale features, such as eddies, are known to constraint the distribution of the zooplankton (Olson, 1991; Huntley et al., 1995; Pinca and Dallot, 1995; Pinca and Huntley, 2000). This role could be related to the factors linked with the hydrological singularities of the frontal zone as stated in the "ergocline theory" (Legendre and Le Fèvre, 1989). Front and eddies are key structures associated within the so-called "ocean triads": enrichment, concentration and retention processes (Bakun, 2006).

In numerous cases, cyclonic eddies or "cold core" eddies, are characterized by an upwelling effect in the central part due to upwelling of nutrient-rich water at the base of the euphotic zone and an increased production of the different constituents of the pelagic food web (Falkowski et al., 1991; Biggs, 1992; Biggs et al., 1997; Ressler and Jochens, 2003; Landry et al., 2008). Centers of anticlonic eddies or "warm core" eddies are in many cases nutrient-depleted and associated with lower biomasses of the different trophic levels (Biggs, 1992; Zimmerman and Biggs, 1999). Occasionally, anticyclonic eddies could be characterized by increased production, especially at the periphery in relation to local dynamic processes (Haury, 1984; Yentsch and David, 1985; Benitez-Nelson and McGillicuddy, 2008; Goldthwait and Steinberg, 2008; Greenan, 2008). We found two different patterns: (1) a high zooplankton biomass near the surface linked to the fluorescence maximum and (2) a high integrated zooplankton biomass related to a larger vertical range and low fluorescence values. These patterns are quite similar to those observed within the Californian coastal eddies, where the distributions of zooplankton were negatively correlated with the chlorophyll concentration within the jet, but positively within the eddy (Huntley et al., 2000). In the Algerian basin (Riandey et al., 2005) small copepod species, like *Paracalanus* or *Clausocalanus*, were also observed with higher abundance at the edge of an anticyclonic eddy. High zooplankton biomass was described in association with the filament water and in the vicinity of island-generated eddies around Gran Canaria (Hernandez-Leon et al., 2001) or on the edge of a warm core eddy of the subtropical convergence in the Southern Ocean (Pakhomov and Perissinotto, 1997). This is in agreement with the physical and biological structures recorded during POMME 2 between C4 and A2 and during POMME 3 for the north edge of the A4 anticyclonic eddy. For the C2 cyclonic eddy (POMME 3), we observed a high phytoplankton biomass coupled with a high biomass of zooplankton. Such enhanced phytoplankton biomass results from the upwelling fluxes of nitrate into the base of the euphotic zone associated with the cyclonic eddy (McGillicuddy and Robinson, 1997). Such high values of zooplankton biomass are obviously linked to richer food resources.

Mesoscale and submesoscale "hot spots" of higher integrated biomasses appear to be linked to phenomena of different natures. At submesoscale, strong integrated zooplankton biomasses associated with low phytoplankton concentrations are directly driven by physics: the peripheral area of anticyclonic eddies is characterized by strong vertical physical gradients and high vertical velocities. At mesoscale of cyclonic eddy, high values of zooplankton biomass associated with high values of fluorescence result from upwelling at the center of the eddy. This dynamic structure must persist long enough to yield development of the upper trophic levels (Ressler and Jochens, 2003). From the point of view of the "ocean triad" (Bakun, 2006), the distribution of the zooplankton biomass seems related to concentration and retention effects at the submesoscale and to enrichment effect at the mesoscale.

Acknowledgments

This work is a contribution to the POMME program funded by the French CNRS (INSU/PROOF program),

IFREMER, Meteo-France, and SHOM agencies and a contribution to MARBEF. The authors would like to thank, in particular, the leaders of the program, Laurent Memery and Gilles Reverdin, the officers and the crew of the SHOM-BO D'Entrecasteaux (POMME 2) and the BSHM Ailette (POMME 3) for their assistance, and the chief scientists of the surveys, Jerome Paillet and Frederic Herpers, for guidance. The comments and remarks of anonymous reviewers improved the manuscript and were greatly appreciated.

References

Albaina, A., Irigoien, X., 2004. Relationships between frontal structures and zooplankton communities along a cross-shelf transect in the Bay of Biscay (1995 to 2003). Marine Ecology Progress Series 284 (65-75).

Ashjian, C.J., Smith, S.L., Flagg, C.N., Wilson, C., 1998. Patterns and occurrence of diel vertical migration of zooplankton biomass in the Mid-Atlantic Bight described by an acoustic Doppler current profiler. Continental Shelf Research 18, 831–858.

Assenbaum, M., Reverdin, G., 2005. Near real-time analyses of the mesoscale circulation during the POMME experiment. Deep Sea Research I 52, 1345–1373.

Bakun, A., 2006. Fronts and eddies as key structures in the habitat of marine fish larvae: opportunity, adaptive response and competitive advantage. Scientia Marina (Barcelona) 70S2, 105–122.

Beaulieu, S.E., Mullin, M.M., Tang, V.T., Pyne, S.M., King, A.L., Twining, B.S., 1999. Using an optical plankton counter to determine the size distributions of preserved zooplankton samples. Journal of Plankton Research 21, 1939–1956.

Benitez-Nelson, C.R., McGillicuddy, D.J., 2008. Mesoscale physical–biological–biogeochemical linkages in the open ocean: an introduction to the results of the E-Flux and EDDIES programs—Preface. Deep-Sea Research Part II—Topical Studies in Oceanography 55, 1133–1138.

Biggs, D.C., 1992. Nutrients, plankton, and productivity in a warm-core ring in the western Gulf of Mexico. Journal of Geophysical Research C Oceans 97 (C2), 2143–2154.

Biggs, D.C., Zimmerman, R.A., Gasca, R., SuarezMorales, E., Castellanos, I., Leben, R.R., 1997. Note on plankton and cold-core rings in the Gulf of Mexico. Fishery Bulletin 95, 369–375.

Claustre, H., Babin, M., Merien, D., Ras, J., Prieur, L., Dallot, S., Prasil, O., Dousova, H., Moutin, T., 2005. Toward a taxon-specific parameterization of bio-optical models of primary production: a case study in the North Atlantic. Journal of Geophysical Research C Oceans 110.

Currie, W.J.S., Claereboudt, M.R., Roff, J.C., 1998. Gaps and patches in the ocean: a one-dimensional analysis of planktonic distributions. Marine Ecology Progress Series 171, 15–21.

Falkowski, P.G., Ziemann, D., Kolber, Z., Bienfang, P.K., 1991. Role of eddy pumping in enhancing primary production in the ocean. Nature 352, 55–58.

Finenko, Z.Z., Piontkovski, S.A., Williams, R., Mishonov, A.V., 2003. Variability of phytoplankton and mesozooplankton biomass in the subtropical and Tropical Atlantic Ocean. Marine Ecology Progress Series 250, 125–144.

Gallienne, C.P., Robins, D.B., Woodd-Walker, R.S., 2001. Abundance, distribution and size structure of zooplankton along a 20 degree west meridional transect of the northeast Atlantic Ocean in July. Deep Sea Research II 48, 4–5.

Giordani, H., Prieur, L., Caniaux, G., 2006. Advanced insights into sources of vertical velocity in the ocean. Ocean Dynamics 56, 513–524.

Goldthwait, S.A., Steinberg, D.K., 2008. Elevated biomass of mesozooplankton and enhanced fecal pellet flux in cyclonic and mode-water eddies in the Sargasso Sea. Deep-Sea Research Part II: Topical Studies in Oceanography 55, 1360.

Grant, S., Ward, P., Murphy, E., Bone, D., Abbott, S., 2000. Field comparison of an LHPR net sampling system and an Optical Plankton Counter (OPC) in the Southern Ocean. Journal of Plankton Research 22, 619–638.

Gray, C.A., Kingsford, M.J., 2003. Variability in thermocline depth and strength, and relationships with vertical distributions of fish larvae and mesozooplankton in dynamic coastal waters. Marine Ecology Progress Series 247, 211–224.

Greenan, B.J.W., 2008. Shear and Richardson number in a mode-water eddy. Deep-Sea Research Part II: Topical Studies in Oceanography 55, 1161.

Halliday, N.C., Coombs, S.H., Smith, C., 2001. A comparison of LHPR and OPC data from vertical distribution sampling of zooplankton in a Norwegian fjord. Sarsia 86, 87–99.

Harris, R.P., 1988. Interactions between diel vertical migration behaviour of marine zooplankton and the subsurface chlorophyll maximum. Bulletin of Marine Science 43, 663–674.

Haury, L.R., 1984. An offshore eddy in the California current system Part IV: plankton distributions. Progress in Oceanography 13, 95–111.

Havens, K.E., 1998. Size structure and energetics in a plankton food web. Oikos 81, 346–358.

Heath, M.R., Dunn, J., Fraser, J.G., Hay, S.J., Madden, H., 1999. Field calibration of the Optical Plankton Counter with respect to *Calanus finmarchicus*. Fisheries Oceanography 8, 13–24.

Herman, A.W., 1988. Simultaneous measurement of zooplankton and light attenuance with a new optical plankton counter. Continental Shelf Research 8, 205–221.

Herman, A.W., 1992. Design and calibration of a new optical plankton counter capable of sizing small zooplankton. Deep-Sea Research 39, 395–415.

Herman, A.W., Cochrane, N.A., Sameoto, D.D., 1993. Detection and abundance estimation of euphausiids using an optical plankton counter. Marine Ecology Progress Series 94, 165–173.

Hernandez-Leon, S., Almeida, C., Gomez, M., Torres, S., Montero, I., Portillo-Hahnefeld, A., 2001. Zooplankton biomass and indices of feeding and metabolism in island-generated eddies around Gran Canaria. Journal of Marine Systems 30, 51–66.

Hopcroft, R.R., 2002. Comparison of plankton size spectra from net tow samples and OPC measurements in marine waters. 17. GLOBEC Report, Tromso.

Huntley, M.E., Gonzalez, A., Zhu, Y., Zhou, M., Irigoien, X., 2000. Zooplankton dynamics in a mesoscale eddy-jet system off California. Marine Ecology Progress Series 201, 165–178.

Huntley, M.E., Zhou, M., Nordhausen, W., 1995. Mesoscale distribution of zooplankton in the California Current in late spring, observed by optical plankton counter. Journal of Marine Research 53, 647–674.

Isla, J.A., Ceballos, S., Huskin, I., Anadon, R., Alvarez-Marques, F., 2004. Mesozooplankton distribution, metabolism and grazing in an anticyclonic slope water oceanic eddy (SWODDY) in the Bay of Biscay. Marine Biology 145, 1201–1212.

Jiang, S.N., Dickey, T.D., Steinberg, D.K., Madin, L.P., 2007. Temporal variability of zooplankton biomass from ADCP backscatter time series data at the Bermuda Testbed Mooring site. Deep-Sea Research I 54, 608–636.

Kato, S., Ito, N., Gunji, K., Aoki, I., Nishida, S., 1997. Small-and meso-scale zooplankton distributions in the Kuroshio area. Report of Japan Marine Science and Technology Center/Kaiyo Kagaku Gijutsu Senta Shiken Kenkyu Hokoku 36, 129–136.

Labat, J.P., Mayzaud, P., Dallot, S., Errhif, A., Razouls, S., Sabini, S., 2002. Mesoscale distribution of zooplankton in the Sub-Antarctic Frontal system in the Indian part of the Southern Ocean: a comparison between optical plankton counter and net sampling. Deep Sea Research I 49, 735–749.

Lampert, W., 1989. The adaptive significance of diel vertical migration of zooplankton. Functional Ecology 3, 21–27.

Landry, M.R., Decima, M., Simmons, M.P., Hannides, C.C.S., Daniels, E., 2008. Mesozooplankton biomass and grazing responses to Cyclone Opal, a subtropical mesoscale eddy. Deep-Sea Research Part II: Topical Studies in Oceanography 55, 1378–1388.

Le Cann, B., Assenbaum, M., Gascard, J.-C., Reverdin, G., 2005. Observed mean and mesoscale upper ocean circulation in the midlatitude northeast Atlantic. Journal of Geophysical Research C Oceans 110, C07S.

Legal, C., Klein, P., Treguier, A., Paillet, J., 2007. Diagnosis of the vertical motions in a mesoscale stirring region. Journal of Physical Oceanography 37, 1413–1424.

Legendre, L., Le Fèvre, J., 1989. Hydrodynamical singularities as control of recycled versus export production in the oceans. In: Berger, W.H., Smetacek, V.S., Wefer, G. (Eds.), Dahlem Workshop on Productivity of the Ocean: Present and Past. John Wiley (Pub), Hoboken, NJ, pp. 49–63.

Liebig, J.R., Vanderploeg, H.A., Ruberg, S.A., 2006. Factors affecting the performance of the optical plankton counter in large lakes: Insights from Lake Michigan and laboratory studies. Journal of Geophysical Research C Oceans 111, C05S.

Lovegrove, T., 1966. The determination of the dry weight of plankton and the effect of various factors on the values obtained. In: Barnes, H. (Ed.), Some Contemporary Studies in Marine Science. George Allen and Unwin, Ltd., London.

McGillicuddy, D.J., Robinson, A.R., 1997. Eddy-induced nutrient supply and new production in the Sargasso Sea. Deep-Sea Research I 44 (8), 1427–1450.

Mullin, M.M., Cass-Calay, S.L., 1997. Vertical distributions of zooplankton and larvae of the Pacific hake (Whiting), *Merluccius productus*, in the California Current system. Reports of California Cooperative Oceanic Fisheries Investigations 38, 127–136.

Olson, D.B., 1991. Rings in the ocean. Annual Review of Earth and Planetary Sciences 19, 283–311.

Osgood, K.E., Checkley, D.M., 1997. Seasonal variations in a deep aggregation of *Calanus pacificus* in the Santa Barbara Basin. Marine Ecology Progress Series 148, 59–69.

Paci, A., Caniaux, G., Gavart, M., Giordani, H., Levy, M., Prieur, L., Reverdin, G., 2005. A high-resolution simulation of the ocean during the POMME experiment: simulation results and comparison with observations. Journal of Geophysical Research C Oceans 110, C07S.

Pakhomov, E.A., Perissinotto, R., 1997. Mesozooplankton community structure and grazing impact in the region of the Subtropical Convergence south of Africa. Journal of Plankton Research 19, 675–691.

Patoine, A., Pinel-Alloul, B., Methot, G., Leblanc, M.J., 2006. Correspondence among methods of zooplankton biomass measurement in lakes: effect of community composition on Optical Plankton Counter and size-fractionated seston data. Journal of Plankton Research 28, 695–705.

Pinca, S., Dallot, S., 1995. Meso- and macrozooplankton composition patterns related to hydrodynamic structures in the Ligurian Sea (Trophos-2 experiment, April–June 1986). Marine Ecology Progress Series 126, 49–65.

Pinca, S., Huntley, M.E., 2000. Spatial organization of particle size composition in an eddy–jet system off California. Deep-Sea Research I 47, 973–996.

Razouls, C., de Bovée, F., Kouwenberg, J., Desreumaux, N., 2005–2008. Diversité et répartition géographique chez les Copépodes planctoniques marins, 〈http://copepodes.obs-banyuls.fr〉.

Remsen, A., Hopkins, T.L., Samson, S., 2004. What you see is not what you catch: a comparison of concurrently collected net, Optical Plankton Counter, and Shadowed Image Particle Profiling Evaluation Recorder data from the northeast Gulf of Mexico. Deep-Sea Research I 51, 129–151.

Ressler, P.H., Jochens, A.E., 2003. Hydrographic and acoustic evidence for enhanced plankton stocks in a small cyclone in the northeastern Gulf of Mexico. Continental Shelf Research 23, 41–61.

Riandey, V., Champalbert, G., Carlotti, F., Taupier-Letage, I., Thibault-Botha, D., 2005. Zooplankton distribution related to the hydrodynamic features in the Algerian Basin (western Mediterranean Sea) in summer 1997. Deep-Sea Research I 52, 2029–2048.

Sameoto, D., Cochrane, N., Herman, A., 1990. Use of multiple frequency acoustics and other methods in estimating copepod and euphausiid abundances. ICES Journal of Marine Science 81, 1–9.

Sheldon, R.W., Paraksh, A., Sutcliffe, W.H., 1972. The size distribution of particles in the ocean. Limnology and Oceanography 17 (3), 327–340.

Sprules, W.G., Bergstroem, B., Cyr, H., Hargreaves, B.R., Kilham, S.S., MacIsaac, H.J., Matsushita, K., Stemberger, R.S., Williams, R., 1992. Non-video optical instruments for studying zooplankton distribution and abundance. Archiv fur Hydrobiologie Beihefte Ergebnisse der Limnologie 36, 45–58.

Sprules, W.G., Jin, E.H., Herman, A.W., Stockwell, J.D., 1998. Calibration of an optical plankton counter for use in fresh water. Limnology and Oceanography 43, 726–733.

Stockwell, J.D., Sprules, J.D., 1995. Spatial and temporal patterns of zooplankton biomass in Lake Erie. ICES Journal of Marine Science 52, 557–567.

Vidal, J., Whitledge, T.E., 1982. Rates of metabolism of Planktonic Crustaceans as related to body weight and temperature of habitat. Journal of Plankton Research 4, 77–84.

Wade, I.P., Heywood, K.J., 2001. Acoustic backscatter observations of zooplankton abundance and behaviour and the influence of oceanic fronts in the northeast Atlantic. Deep-Sea Research II 48, 899–924.

Wieland, K., Petersen, D., Schnack, D., 1997. Estimates of zooplankton abundance and size distribution with the Optical Plankton Counter (OPC). Archive of Fishery and Marine Research = Archiv für Fischerei- und Meeresforschung 45, 271–280.

Woodd-Walker, R.S., Gallienne, C.P., Robins, D.B., 2000. A test model for optical plankton counter (OPC) coincidence and a comparison of OPC-derived and conventional measures of plankton abundance. Journal of Plankton Research 22, 473–483.

Yebra, L., Almeida, C., Hernandez-Leon, S., 2005. Vertical distribution of zooplankton and active flux across an anticyclonic eddy in the Canary Island waters. Deep-Sea Research I 52, 69–83.

Yentsch, C.S.P., David, A., 1985. Rorary motions and convection as a means of regulating primary production in warm core rings. Journal of Geophysical Research 90, 3237–3248.

Zimmerman, R.A., Biggs, D.C., 1999. Patterns of distribution of sound-scattering zooplankton in warm- and cold-core eddies in the Gulf of Mexico, from a narrowband acoustic Doppler current profiler survey. Journal of Geophysical Research C Oceans 104, 5251–5262.